Supplementary Material

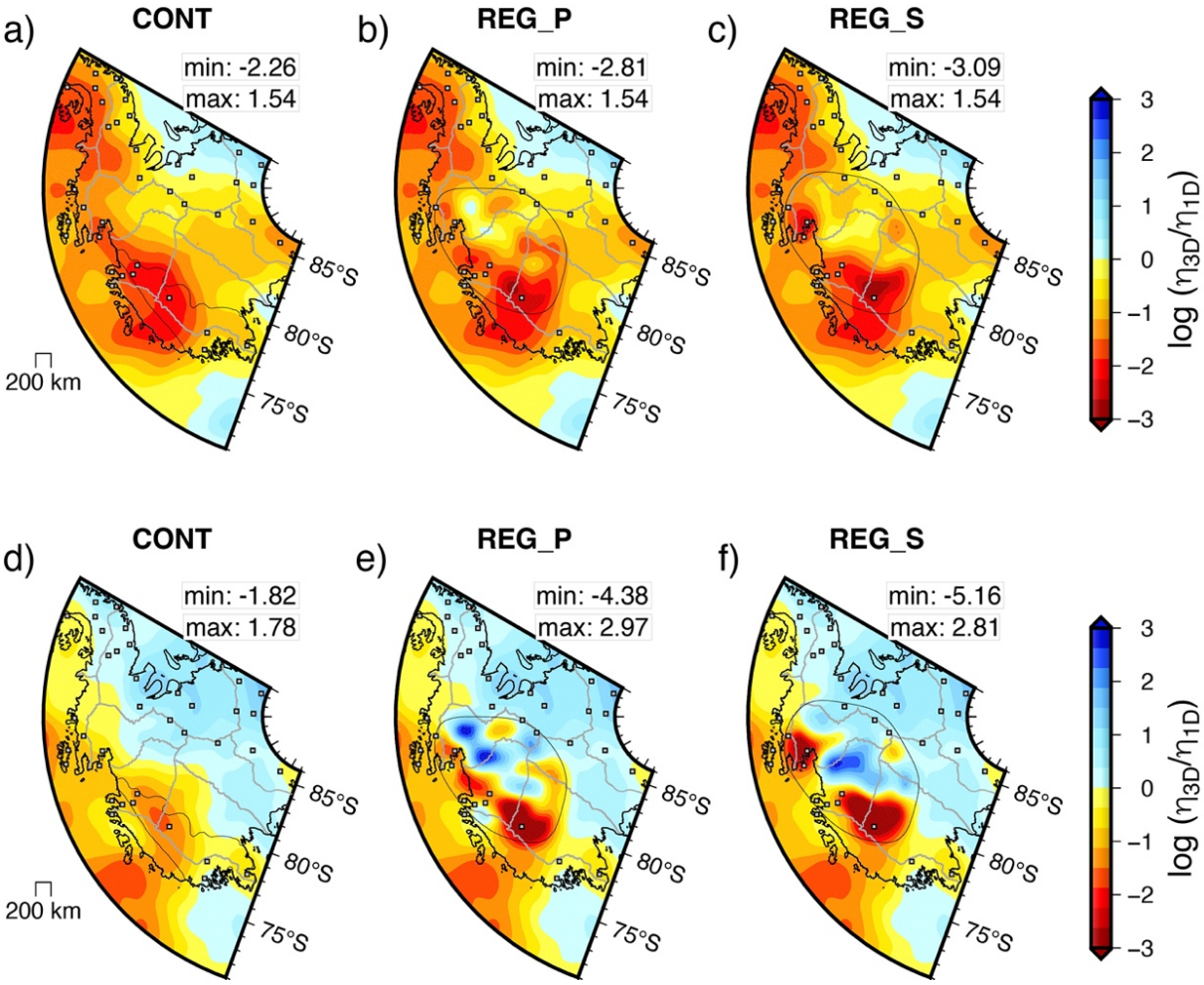

Figure S1. Depth slices through 3-D viscosity models at (a-c) 100 km depth and (d-f) 200 km depth. Depth slices are plotted as logarithmic viscosity perturbation maps like in Figure 1. The location of the maps are outlined in Fig. 1b.

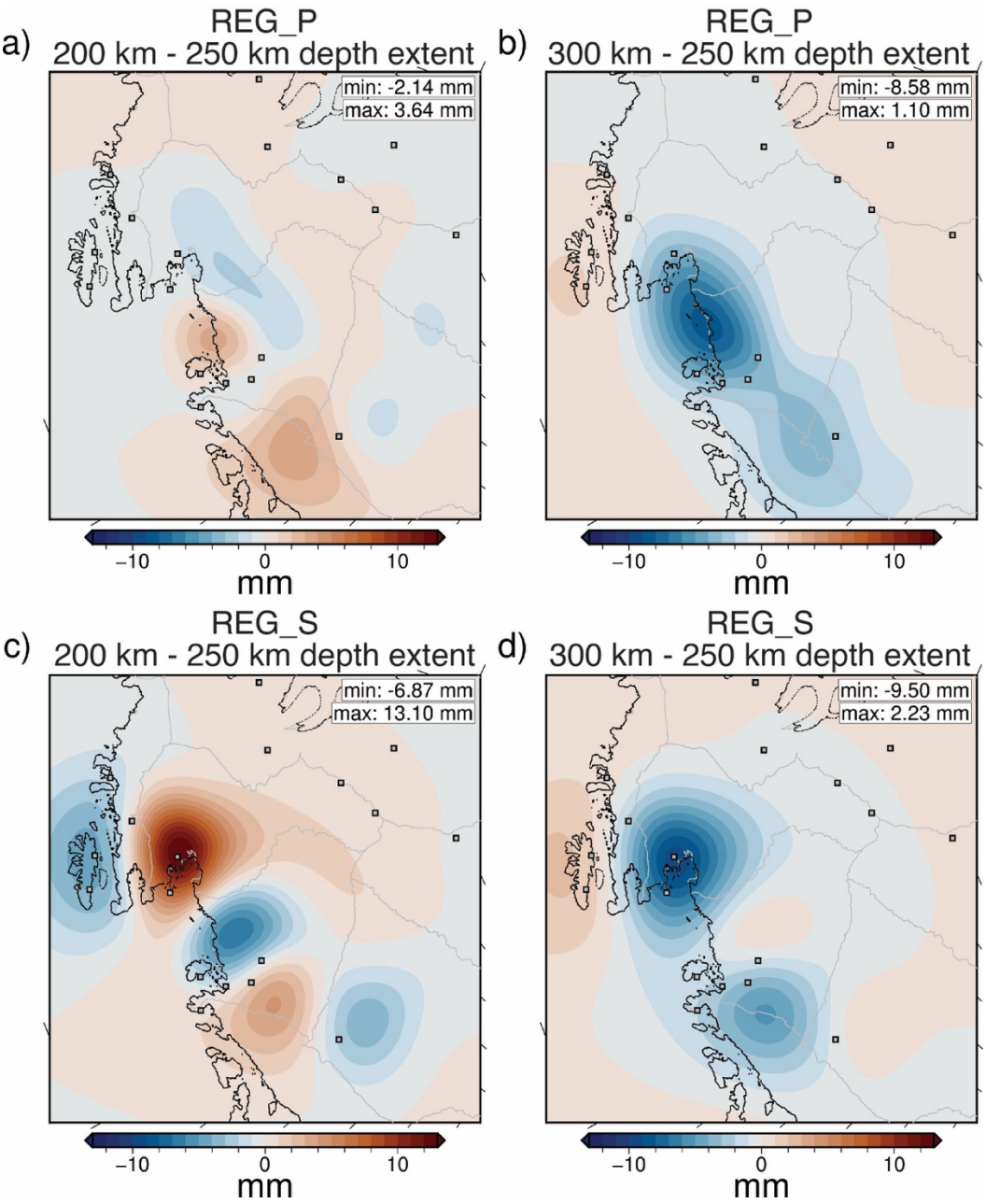

Figure S2. Difference in relative sea level predicted in simulations with ICE-25 for Earth models in which the regional body-wave tomography models were inserted in the ANT-20 and GLAD-M25 composite models over different depth extents (i.e., P- and S-wave models inserted to 200 km, 250 km, and 300 km depths). Note, the regional body wave model is inserted from the base of the lithosphere to 250 km depth for the REG_P and REG_S viscosity models. (a-b) Difference in predicted relative sea level between simulations adopting viscosity models where the P-wave model extends to (a) 200 km depth and (b) 300 km depth and the REG_P viscosity model. (c-d) Difference in predicted relative sea level between simulations adopting viscosity models where the S-wave model extends to (a) 200 km depth and (b) 300 km depth and the REG_S viscosity model.

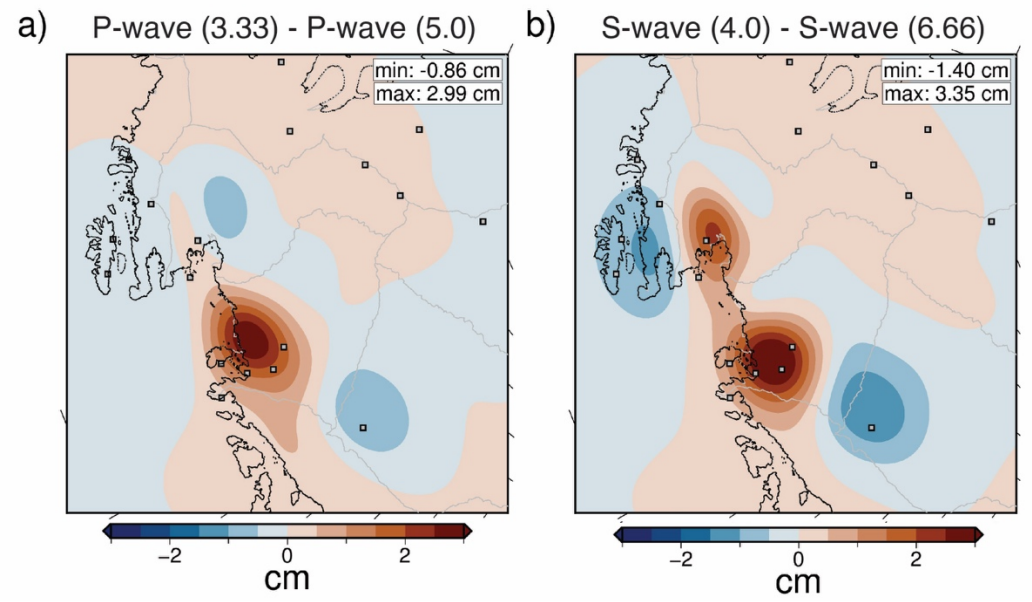

Figure S3. Impact of assumptions made in the construction of regional viscosity models on relative sea level predictions: (a) Difference in predicted relative sea level for simulations adopting a viscosity model constructed assuming high-end amplitude recovery in the P-wave model (i.e., 30% amplitude recovery) and the REG_P viscosity model. (b) Difference in predicted relative sea level for simulations adopting a viscosity model constructed assuming high-end amplitude recovery in the S-wave model (i.e., 25% amplitude recovery) and the REG_S viscosity model. All simulations shown here adopt the ICE-25 ice history. From this comparison, we find a maximum difference of 2.99 cm and 3.35 cm between relative sea level predictions adopting the viscosity models constructed accounting for high-end and low-end amplitude in the P-wave and S-wave models, respectively. Therefore, the adopted amplitude scaling factor only contributes up to ~7% of the total relative sea level prediction. Although there is some discrepancy in the predicted magnitude of relative sea level, a similar spatial pattern in relative sea level predictions is produced in simulation adopting the low- and high-end P- and S-wave models, respectively. The similarity in the spatial pattern of GIA predictions between models scaled for high- and low-end amplitude recovery indicates that the adopted scaling factor does not have the largest control on model predictions; instead, the spatial pattern of upper mantle viscosity has the greater impact on GIA predictions. Therefore, given the relatively minor impact of chosen amplitude scaling factor on GIA model predictions, we will focus on simulations adopting the REG_P and REG_S viscosity models throughout the main text.

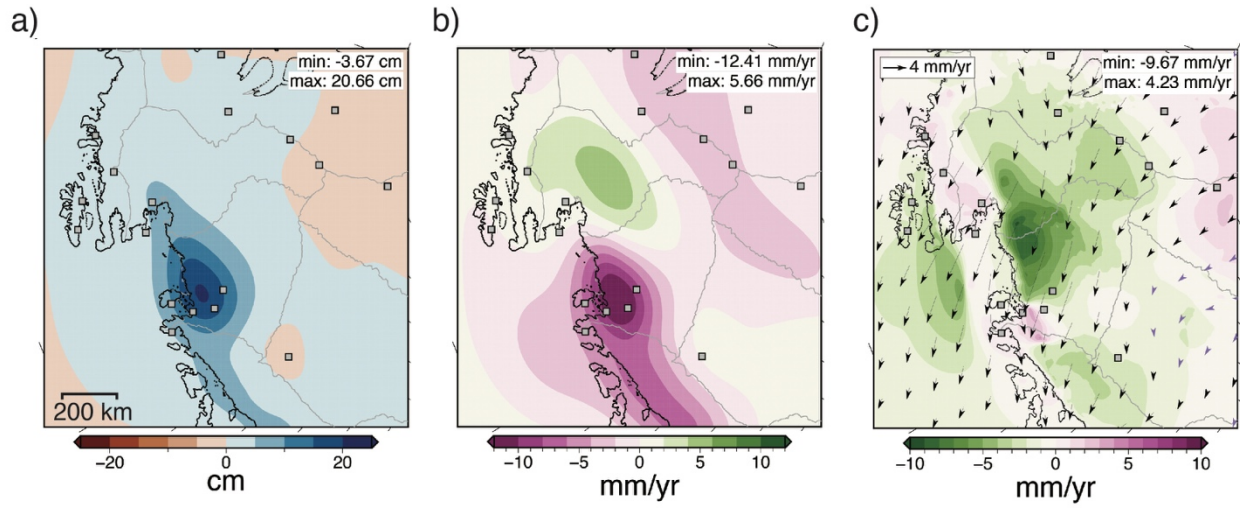

Figure S4. Difference in (a) relative sea level, (b) vertical crustal motion, and (c) horizontal crustal motion predictions between simulations adopting the 1D viscosity model versus the CONT viscosity model with the ICE-125 ice model.

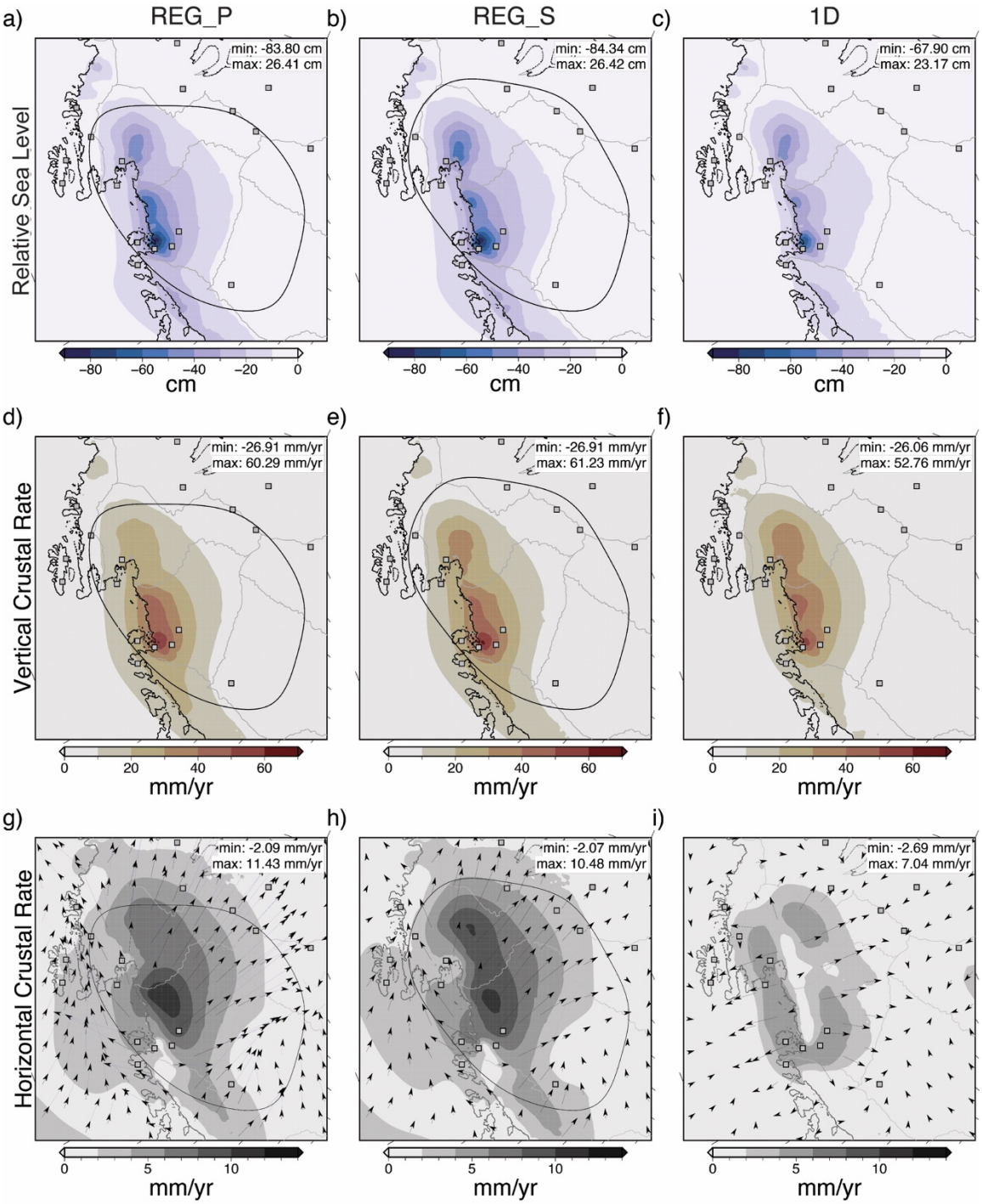

Figure S5. (a-c) Relative sea level predictions for simulations adopting the ICE-125 ice model and the (a) REG_P, (b), REG_S, and (c) 1D viscosity models. (d-f) Vertical crustal motion rates predicted at the end of simulations adopting the ICE-125 ice model and the (d) REG_P, (e) REG_S, and (f) 1D viscosity models. (g-i) Horizontal crustal motion rates predicted at the end of simulations adopting the ICE-125 ice model and the (g) REG_P, (h) REG_S, and (i) 1D viscosity models.

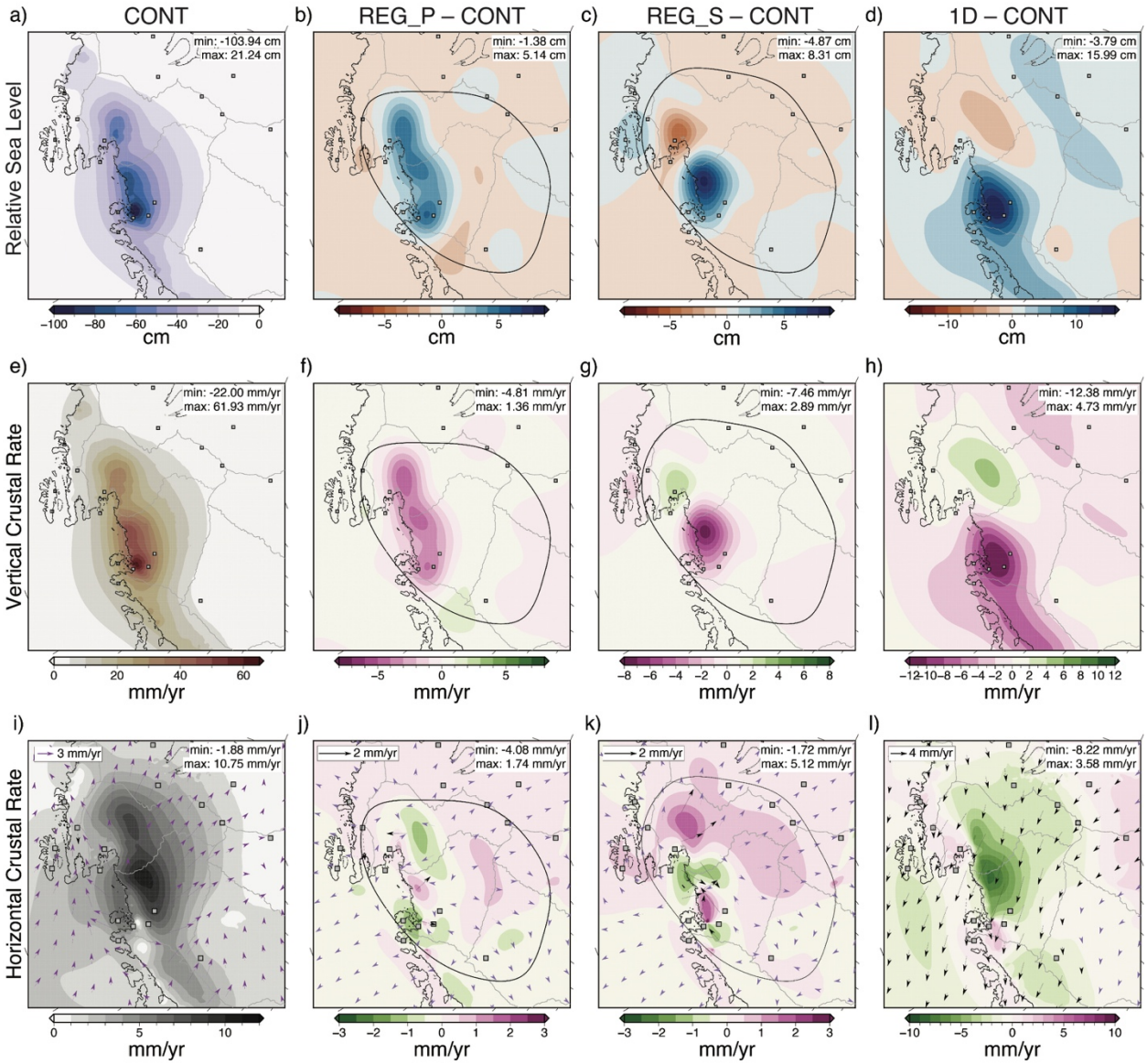

Figure S6. Influence of regional upper mantle structure on predictions of sea level and crustal motion rates for modern ice loading (ICE-25). (a) Relative sea level change in centimeters for a GIA model simulation with the CONT viscosity model and the ICE-25 ice model. (b-d) Difference in predicted relative sea level change between the (b) REG_P, (c) REG_S, (d) 1D and CONT viscosity models. (e) Vertical crustal motion rate predicted at the end of a simulation adopting the CONT viscosity model and the ICE-25 model. (f-h) Difference in predicted vertical crustal motion rates between the (f) REG_P, (g) REG_S, and (h) 1D viscosity models and the CONT viscosity model at the end of simulations with the ICE-25 ice model. (i) Horizontal crustal motion rate predicted at the end of the simulation adopting the CONT viscosity model and the ICE-25 ice model. (j-l) Difference in horizontal crustal motion rates after 25 years of loading (ICE-25) between the (j) REG_P, (k) REG_S, and (l) 1D and CONT viscosity models. (j-l) Vectors show the difference in predicted direction and magnitude of horizontal crustal motion rates between the respective panel's viscosity model and the CONT viscosity model. Black and purple arrows correspond to locations with horizontal crustal motion rates ≥1 mm/year and <1 mm/year, respectively.

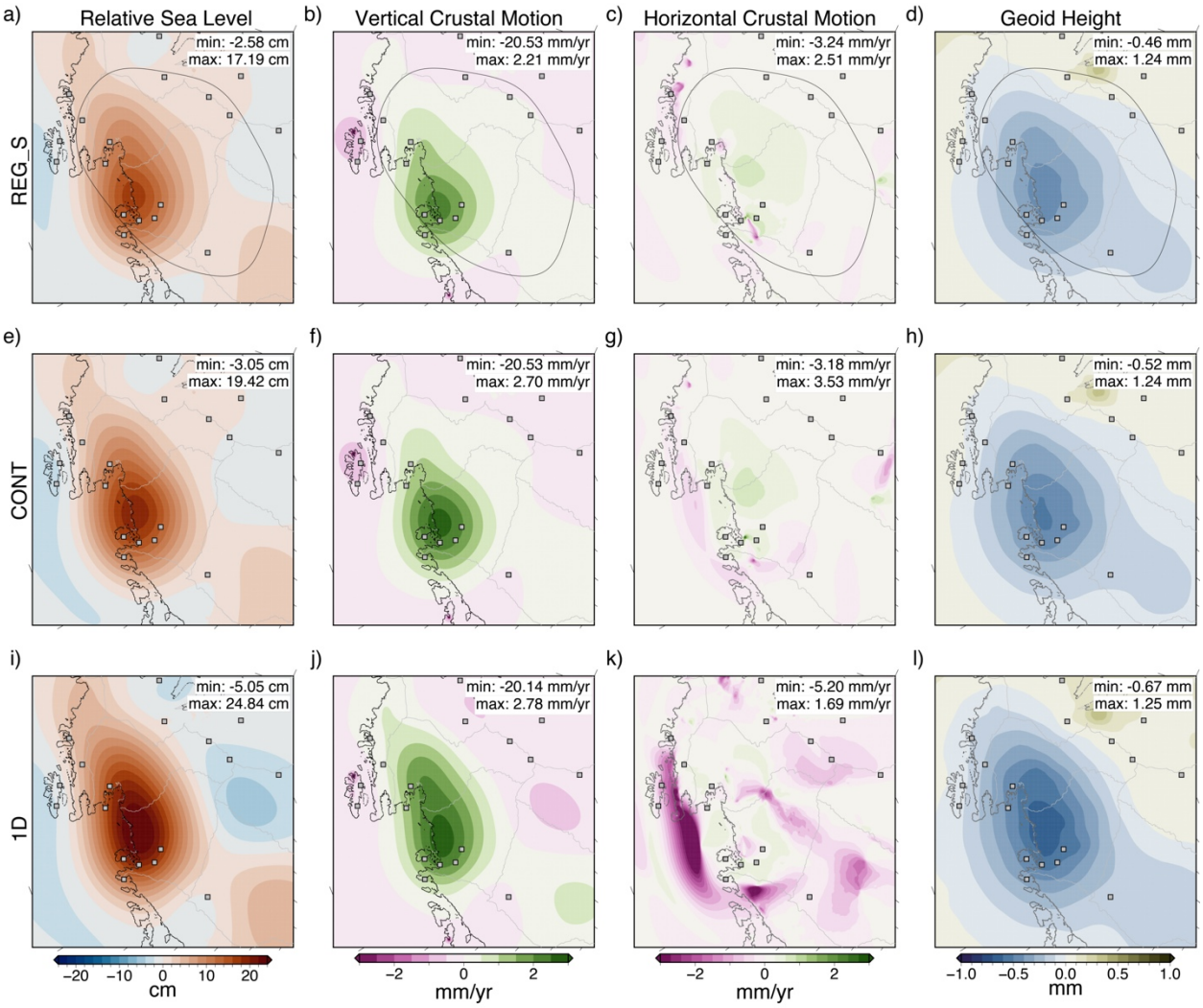

Figure S7. Impact of ice history length (ICE-125 versus ICE-25) on model predictions for the (a-d) REG_S, (e-h) CONT, and (i-l) 1D Earth models. Differences in relative sea level predictions for 1992-2017 are shown in the first column. Differences in vertical and horizontal crustal motion predictions at the end of the simulation in 2017 are in the second and third columns. Differences in geoid height predictions for 1992 – 2017 are in the fourth column.

Table S1. Observed and predicted crustal rates at GPS sites

			Observed						
			Vertical (mm/yr)	Horizontal (mm/yr)			Vertical Error (mm/yr)	Horiz. Error (mm/yr)	
Station	Latitude	Longitude		East	North	Total		Sigma E	Sigma N
BACK	-74.43044137	-102.4781855	15.22	0.21	4.47	4.47	0.11	0.04	0.03
BERP	-74.54593593	-111.8845842	26.67	1.22	9.43	9.51	0.12	0.06	0.05
INMN	-74.82086547	-98.88046683	31.81	-2.55	7.22	7.66	0.38	0.2	0.21
MCRG	-73.66779881	-94.64632176	2.03	-1.09	1.4	1.77	1.2	0.38	0.36
MRTP	-74.18040529	-115.1021358	14.12	0.4	4.17	4.19	0.57	0.2	0.16
MTAK	-76.315041329	-112.800012	43.94	-2.38	-7.64	8	0.89	0.21	0.2
SDLY	-77.13531279	-125.9745777	-2.15	2.78	1.46	3.14	0.17	0.03	0.05
SLTR	-75.09815674	-113.8795515	49.65	-3.23	10.8	11.28	1	0.21	0.2
TOMO	-75.80186751	-114.6619037	50.49	-5.86	-2.74	6.47	0.46	0.16	0.2

Predicted

	REG_P, ICE-125					REG_P, ICE-25			
	Vertical (mm/yr)	Horizontal (mm/yr)				Vertical (mm/yr)	Horizontal (mm/yr)		
Station		East	North	Total			East	North	Total
BACK	14.69	3.87	0.98	3.99		13.88	3.47	1.01	3.61
BERP	24.53	3.12	3.59	4.76		22.58	2.89	3.55	4.58
INMN	19.39	3.56	0.71	3.64		18.62	3.21	0.81	3.31
MCRG	9.52	2.48	0.87	2.63		9.45	2.33	0.83	2.48
MRTP	18.95	1.28	2.03	2.4		17.7	1.27	1.98	2.36
MTAK	30.04	1.82	-7.81	8.01		28.2	1.66	-7.19	7.38
SDLY	3.48	0.78	-2.23	2.37		3.43	0.69	-2.14	2.25
SLTR	40.55	-0.41	3.85	3.87		38.34	-0.43	4.03	4.06
TOMO	37.02	-1.53	-5.15	5.37		35.03	-1.48	-4.69	4.91

	REG_S, ICE-125					CONT, ICE-125			
	Vertical (mm/yr)	Horizontal (mm/yr)				Vertical (mm/yr)	Horizontal (mm/yr)		
Station		East	North	Total			East	North	Total
BACK	16.09	3.58	0.96	3.71		15.17	3.93	1.38	4.16
BERP	24.4	4.04	3.57	5.39		25.93	3.39	4.49	5.63
INMN	24.04	3.11	0.78	3.21		21.44	3.25	1.48	3.57
MCRG	8.76	2.37	0.46	2.42		9.22	2.18	0.56	2.25
MRTP	19.32	1.52	2.32	2.78		19.54	1.14	2.5	2.75
MTAK	30.35	3.30	-7.56	8.25		32.85	1.71	-8.06	8.24
SDLY	2.83	1.24	-2.19	2.51		3.03	1.29	-2.1	2.46

SLTR	41.58	1.21	4.26	4.43		43.76	-0.08	4.81	4.81
TOMO	38.64	-0.14	-5.10	5.1		40.57	-1.71	-5.37	5.63

	1D, ICE-125			
	Vertical (mm/yr)	**Horizontal (mm/yr)**		
Station		**East**	**North**	**Total**
BACK	15.3	-0.29	3.92	4.33
BERP	20.05	0.07	4.77	5.2
INMN	22.54	-0.9	4.4	4.8
MCRG	11.08	-0.26	2.35	2.58
MRTP	15.26	-1.2	3.2	3.75
MTAK	24.72	-2.11	-3.77	4.78
SDLY	3.11	-0.11	-0.76	0.66
SLTR	34.22	-2.74	5.02	6.01
TOMO	29.99	-4.09	-2.83	5.44